6

Monitoring Integrated Activity of Individual Neurons Using FRET-Based Voltage-Sensitive Dyes

Kevin L Briggman, William B. Kristan, Jesús E. González, David Kleinfeld, and Roger Y. Tsien

6.1 INTRODUCTION

Fluorescence resonance energy transfer (FRET) is a physical dipole–dipole coupling between the excited state of a donor fluorophore and an acceptor chromophore that causes relaxation of the donor to a non-fluorescent ground state, which excites fluorescence in the acceptor. Initially described by Förster (1948), FRET has been extensively reviewed (Stryer 1978; Clegg 1995; Selvin 2000; Lakowicz 2006). In practical terms, the efficiency of FRET depends on the properties of the chromophores and the distance between them, measured as the Förster radius (R_o): the distance between the donor and the acceptor at which half the energy is transferred. The magnitude of R_o depends on the donor quantum yield and the spectral overlap between the donor emission and the acceptor absorbance spectra. For commonly used synthetic FRET pairs, R_o values range from 2 to 8 nm (Wu and Brand 1994). FRET efficiency is inversely proportional to the sixth power of the donor and acceptor distance, providing a sensitive readout of intermolecular distances near R_o. Experimentally, FRET is measured either as the decrease in the lifetime or intensity of donor fluorescence after the addition of acceptor, or as the increase in acceptor fluorescence after the addition of donor. Because typical R_o values are similar to protein and membrane dimensions, FRET has proven useful in a wide variety of biochemical and cellular applications to investigate protein–protein interactions, protein and DNA conformational analysis, and membrane topography (Stryer 1978; Clegg 1995; Selvin 2000; Lakowicz 2006). Furthermore, with the advent of a large variety of fluorescent protein color variants, FRET has become a natural method to probe cellular biochemistry (Piston and Kremers 2007). Here, we review how FRET probes have been used to measure cellular membrane potentials.

Voltage-sensitive dyes (VSDs) based upon FRET are composed of two molecules, with either the donor or acceptor being a hydrophobic anion introduced into the plasma membrane acting as the voltage sensor by translocating between the energy minima at the intracellular and extracellular membrane–water interfaces (Fig. 6.1A) (Gonzalez and Tsien 1995). When the transmembrane potential changes, the hydrophobic anion redistributes as an exponential function of the potential according to the Nernst equation. A second impermeant fluorophore is attached to one face of the membrane where it can undergo FRET with the mobile molecule, in proportion to the distance between the two molecules. When the impermeant fluorophore is bound to the extracellular membrane surface and the cell is at its normal (negative) resting potential, the anions are predominately near the extracellular face of the membrane, so that the two molecules produce efficient FRET. When the membrane depolarizes, for whatever reason, the anions equilibrate at a higher density at the intracellular membrane surface, thereby decreasing FRET. When both molecules are fluorescent, all increases in the acceptor emission are at the expense of the donor emission, and vice versa (Fig. 6.2A, B), thus providing a ratiometric signal of the membrane potential change.

FRET-based dyes are sometimes called "slow" dyes, which is true relative to electrochromic dyes that have typical response times of a few microseconds (Ebner and Chen 1995; Baker et al. 2005), but FRET dye time constants actually span a large range, from 400 µs to 500 ms, depending on the properties of the mobile anion. While not the fastest, FRET dyes have yielded some of the largest observed fractional fluorescence changes, ranging from 10–20% per 100 mV in intact tissue (Cacciatore et al. 1999) to 100–300% per 100 mV in isolated cells (Gonzalez and Maher 2002).

Following a brief account of the development of FRET VSDs, we discuss their temporal resolution, sensitivity, and phototoxicity. We then present examples of how these dyes have been used to image neurons. Finally, we provide detailed staining protocols as a reference and starting points for use in other systems.

6.2 DEVELOPMENT OF FRET DYE PAIRS

Gonzalez and Tsien (1995) were first to image voltage-dependent responses from a FRET-based VSD. They used negatively charged hydrophobic oxonol derivatives, bis-(1,3-dialkyl-2-thiobarbiturate)-trimethineoxonol, DiSBAC$_x$(3), where x refers to the number of

Kevin L. Briggman • Department of Biomedical Optics, Max Planck Institute for Medical Research, Jahnstrasse 2969120, Heidelberg, Germany
William B. Kristan • Neurobiology Section, Division of Biological Sciences, University of California, San Diego 9500 Gilman Drive, La Jolla, CA 92093-0357, USA
Jesús E. González • 6468 Wayfinders Court, Carlsbad, CA 92011, USA
David Kleinfeld • Department of Physics, University of California, San Diego, 9500 Gilman Drive, La Jolla, CA 92093-0374, USA
Roger Y. Tsien • Department of Pharmacology, Howard Hughes Medical Institute, University of California, San Diego 310 George Palade Labs, 9500 Gilman Drive, La Jolla, CA 92093-0647, USA

M. Canepari and D. Zecevic (eds.), *Membrane Potential Imaging in the Nervous System: Methods and Applications*,
DOI 10.1007/978-1-4419-6558-5_6, © Springer Science+Business Media, LLC 2010

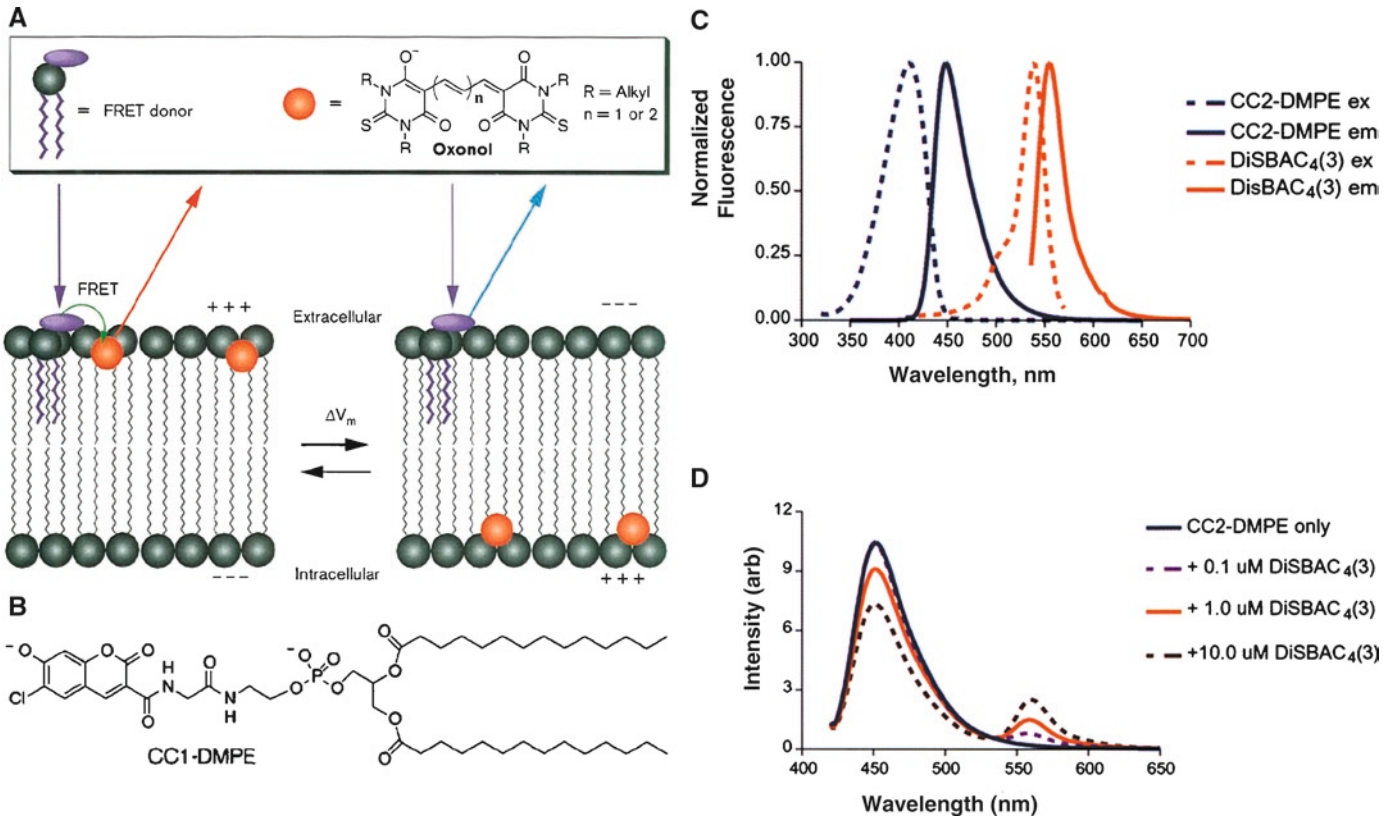

FIGURE 6.1. Properties of a FRET VSD dye pair. (A) Most FRET VSDs incorporate an immobile donor (*purple*) and a mobile anion (*orange*). A variety of molecules can be used for this purpose. Oxonol derivatives are a versatile choice for the mobile anion. When the donor fluorophore is excited (*purple arrow*), it will either emit blue photons when the mobile anion is near the intracellular surface of the membrane (*blue arrow* in the right diagram) or produce FRET when the mobile ion is near the extracellular surface (*orange arrow* in the left diagram). (B) The structure of a FRET donor, CC1-DMPE, a coumarin-labeled phospholipid. (C) The excitation and emission spectra for the CC2-DMPE and DiSBAC$_4$(3) dye pair. The overlap between donor emission and acceptor excitation determines the FRET efficiency; the more complete the overlap, the more efficient is FRET. The emission spectra for these two dyes are well separated, making them a useful dye pair. (D) Emission spectra of the two dyes as DiSBAC$_4$(3) was loaded into cell membranes. Increased concentrations of DiSBAC$_4$(3) progressively quenched the CC2-DMPE emission. Panels (A) and (B) are reproduced with permission from Gonzalez and Tsien (1997), and panels (C) and (D) are reproduced with permission from Gonzalez and Maher (2002).

carbons on the alkyl group and 3 refers to the number of polymethine carbons), as the mobile voltage sensor. Negatively charged oxonol molecules such as DiSBAC$_2$(3) and bis-(1,3-dibutylbarbituric acid) trimethine oxonol [DiBAC$_4$(3)] have previously been used as redistribution VSDs (Rink et al. 1980; Ebner and Chen 1995). They move between intracellular and extracellular compartments in response to membrane potential changes with very slow kinetics (seconds to minutes). An impermeant oxonol has also been used as a fast absorption dye (Grinvald et al. 1981; Wu et al. 1994b; Momose-Sato et al. 1999). Fluorescence changes result from the fact that oxonols are non-fluorescent in water but are highly fluorescent in hydrophobic environments such as membranes. An anion was chosen, rather than a cation, to take advantage of the dipole potential generated from the polar lipid head-groups, presumably from the ester carbonyl groups, which greatly speeds anion translocation. The rate differences for isostructural borates and phosphonium ions are orders of magnitude faster for the negatively charged borates (Flewelling and Hubbell 1986). Although the mobile anion can in principle serve as either the FRET donor or acceptor, it is most commonly used as the FRET acceptor. As discussed below, there are theoretical and practical advantages for the reverse configuration. The FRET donor was initially chosen to be fluorescein-labeled wheat germ agglutinin (FL-WGA) that bound to *N*-acetylglucosamine groups on the extracellular face of plasma membranes (Gonzalez and Tsien 1995). The same study showed that using longer chain alkyl groups not only increased the oxonol hydrophobicity but also resulted in faster membrane translocation speed, which improved the FRET temporal resolution, presumably by burying the oxonol deeper into the low dielectric region of the membrane. The optimal chain length was 6 and DiSBAC$_6$(3) had a translocation time constant ~2 ms.

The original dye pair was improved by replacing FL-WGA with a fluorescent phospholipid, *N*-(6-chloro-7-hydroxy-2-oxo-2H-l-benzopyran-3-carboxamidoacetyl)-dimyristoylphosphatidyl ethanolamine [CC1-DMPE] (Gonzalez and Tsien 1997) (Fig. 6.1B). A second chlorocoumarin phospholipid CC2-DMPE is commercially available from Life Technologies (formerly Invitrogen); it has similar properties to CC1-DMPE. The coumarin has a high quantum yield (indistinguishable from 1) and makes an excellent FRET partner with trimethine thiobarbiturate oxonols. The fluorescence emission maxima are separated by 100 nm (Fig. 6.1C), thus enabling efficient collection of both donor and acceptor photons. Another key property of chlorocoumarin phospholipid donors is that they have two negative charges at physiological pH. This is important because it anchors the fluorescent head-group at the extracellular surface and prevents probe translocation across the plasma membrane which would greatly degrade the voltage-sensitive FRET signal. In addition to the phosphate charge, the

chloro-group reduces the pK_a of the hydroxy coumarin (Fig. 6.1B) to ~5, which results in a second negative charge at physiological pH. A pyrene phospholipid has also been developed as a pH insensitive FRET donor that is compatible with low pH conditions used to activate acid-sensitive channels (Maher et al. 2007). The use of a phospholipid placed the donor fluorophore closer to the membrane–water interface, thereby decreasing the minimal distance between donor and acceptor, which may account for the increased voltage sensitivity with the fluorescent impermeant phospholipid (Gonzalez and Tsien 1997). In addition to the original oxonol dye DiSBAC$_6$(3), longer wavelength pentamethine oxonols were developed (the oxonol shown in Fig. 6.1A has $n = 2$) (Gonzalez and Tsien 1997). Increasing the polymethine chain length from trimethine oxonol [DiSBAC$_6$(3)] to pentamethine oxonol [DiSBAC$_6$(5)] increases charge delocalization, thereby further lowering the activation energy for translocation. This change yielded a time constant for DiSBAC$_6$(5) of ~0.4 ms.

The FRET-based VSD strategy has more recently been used in hybrid voltage sensor systems, incorporating fast anions, such as dipicrylamine (DPA) or DiBAC$_4$(5), with a genetically expressed donor fluorophore such as farnesylated enhanced GFP (eGFP-F) (Chanda et al. 2005). DPA is an absorption dye that does not fluoresce; it serves only to quench the fluorescence of the donor molecule when FRET occurs. The structure of the donor fluorophore has been additionally modified to be able to record action potentials (DiFranco et al. 2007; Sjulson and Miesenbock 2008).

Together these developments and optimizations of FRET-based VSDs demonstrate the versatility in choosing the donor and acceptor for a variety of applications. Most importantly, the source of the voltage sensitivity is well understood making the rational design of future improvements possible.

6.3 RESPONSE TIME OF FRET INDICATORS

Because the lifetime of FRET is short, on the order of nanoseconds, the time constant of FRET VSDs is determined by the rate that the hydrophobic anion equilibrates across the membrane when the membrane potential changes (Gonzalez and Tsien 1995). As mentioned above, increasing the length of the alkyl side chains of oxonol increases hydrophobicity and therefore increases its response speed. For example, DiSBAC$_2$(3) and DiSBAC$_6$(3) have time constants of 500 ms and 2 ms, respectively (Gonzalez and Maher 2002). However, increased hydrophobicity comes at the cost of reduced aqueous solubility, limiting loading concentrations (Table 6.1). Using pluronic F-127 and β-cyclodextrin brings the more hydrophobic oxonols into

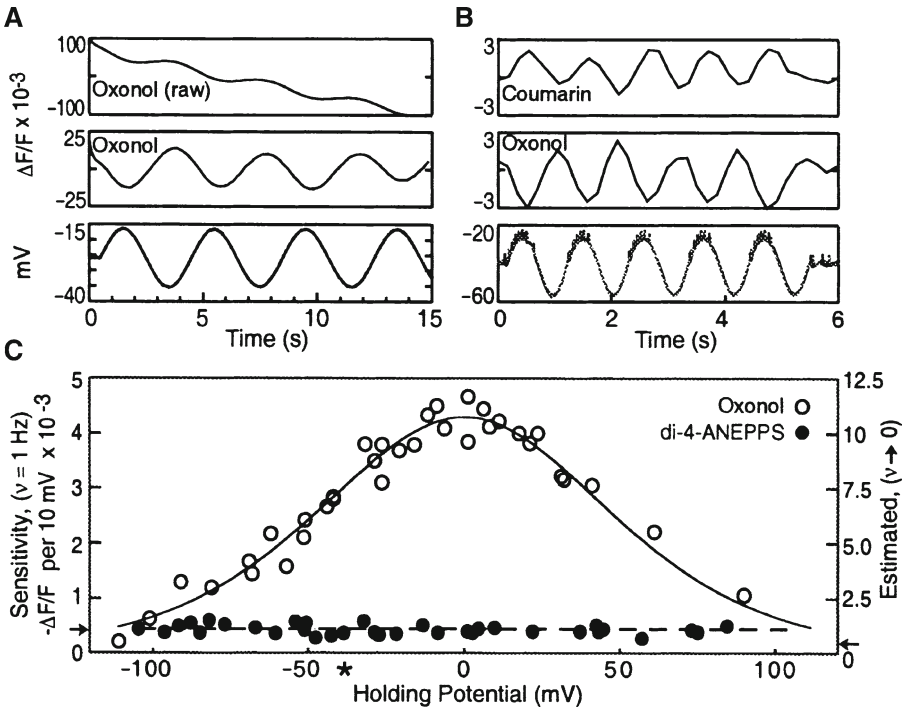

FIGURE 6.2. Voltage-dependent signals of FRET VSDs. (A) Leech neurons were voltage clamped and the membrane potentials was sinusoidally varied about a holding potential (bottom trace). The raw oxonol trace (top trace) was filtered (middle trace) to remove the slow bleaching artifact visible in the top trace. (B) Sequential recordings of the coumarin and oxonol emission wavelengths to the same sinusoidally varying intracellular stimulus demonstrating that, because the two dyes produce out-of-phase signals, the sensitivity can be enhanced by measuring the ratio of the two signals. (C) The sensitivity of the FRET signal is a function of the membrane potential measured at various holding potentials. The data are well fit by the expected redistribution of oxonol across the membrane during changes in membrane potential (*open circles*). FRET VSDs in leech ganglia are significantly more sensitive than other VSDs such as di-4-ANEPPS (*filled circles*). Panels reproduced with permission from Cacciatore et al. (1999).

TABLE 6.1. Oxonol Derivatives that can be Used as the Mobile Anion and Their Associated Time Constants and Measured Sensitivities

	Commercially Available	Pluronic Loading	λ_{ex} (nm)	λ_{em} (nm)	T_c (ms)	V_m sensitivity % ΔR per mV
DiSBAC$_2$(3)	Yes	Optional	540	560	500	1–3
DiSBAC$_4$(3)	Yes	Suggested	540	560	20	0.6–1
DiSBAC$_6$(3)	No	Required	540	560	2	0.4–0.8
DiSBAC$_2$(5)	No	Optional	640	660	50	0.5–2[a]
DiSBAC$_4$(5)	No	Suggested	640	660	2	<0.4[a]
DiSBAC$_6$(5)	No	Required	640	660	0.40	<0.2[a]

Table reproduced with permission from Gonzalez and Maher (2002)
[a]Not optimized

contact with cells, which helps to load these dyes. The optimal loading concentration for any FRET acceptor should be high enough to quench a large fraction of donor fluorescence (Fig. 6.1D), to be sure that the acceptor is in the same membrane as the donor, but not so high that it adds a large capacitance to the cell membranes. In practice, loading concentrations for $DiSBAC_2(3)$ and $DiSBAC_4(3)$ oxonol should not exceed 20 μM (Cacciatore et al. 1999), although the effect of voltage-sensitive anions on membrane capacitance should always be assayed with intracellular electrical recordings when applied to a new preparation. For example, concentrations of DPA above 2 μM inhibit action potentials in *Drosophila* neurons (Sjulson and Miesenbock 2008).

Increasing charge delocalization by changing the polymethine chain length of oxonol from trimethine to pentamethine increases the translocation speed 2- to 20-fold (Table 6.1). $DiSBAC_6(5)$ has a time constant of ~0.4 ms compared to 2 ms for $DiSBAC_6(3)$ (Gonzalez and Tsien 1997). The time constant of DPA used in hybrid voltage sensor systems is ~0.5 ms (Chanda et al. 2005). All the quoted oxonol time constants were measured at 20°C; increasing temperature to 29°C speeds up the translocation rate two- to threefold (Gonzalez and Tsien 1995).

6.4 SENSITIVITY OF FRET INDICATORS

The efficiency of FRET depends on the Förster distance, R_0, the distance at which FRET is 50% efficient. To ensure that FRET occurs selectively between the donor and acceptor on the same side of the membrane, ideally R_0 needs to be less than the width of the intra- and extracellular binding sites of the membrane (3–5 nm). One way to decrease R_0 while maintaining strongly absorbing fluorophores with high quantum yield is to decrease spectral overlap between the donor emission and acceptor excitation spectra (Fig. 6.1C). For the original FL-WGA and oxonol pairs, the measured fluorescence changes were more than 20-fold less than expected from a Nernst equation-based mechanism, meaning the voltage sensitivity of oxonol was not efficiently transduced into a usable FRET signal (Gonzalez and Tsien 1995). Bringing the donor closer to the membrane and decreasing the donor and acceptor spectral overlap, by replacing FL-WGA with CC1-DMPE reduced the minimal distance between the two fluorophores, increasing FRET efficiency and, thereby, the sensitivity of the measurement.

The modification of $DiSBAC_6(3)$ to $DiSBAC_6(5)$, in addition to increasing translocation speed, shifted the absorption spectrum of oxonol to longer wavelengths by 100 nm (Gonzalez and Tsien 1997). The decreased overlap between the CC1-DMPE emission and $DiSBAC_6(5)$ absorption spectra further reduced R_0 to 3.7 nm. The reduction in FRET due to the decreased spectral overlap is compensated by an increase in FRET selectivity for oxonol molecules near the extracellular face of the membrane. Separating the spectral overlap between donor and acceptor has the added benefit of limiting inadvertent illumination of the acceptor. Unfortunately, the pentamethine oxonols bleach much faster than trimethine oxonols and this imposes a significant limitation on using this faster oxonol.

The voltage sensitivity of FRET VSDs is maximal when the acceptor can quench most of the donor emission when the two molecules are in close proximity. Thus, the stoichiometry of the loading concentrations of the donor and acceptor needs to be optimized depending on cell type. In theory, it is preferable to have the mobile anion serve as FRET donor because efficient FRET relies on high acceptor concentrations. Lowering oxonol concentration limits photodamage, electrostatic repulsion between oxonol molecules, and the capacitive load on cells. A proof of this principle used $DiSBAC_6(3)$ as the mobile FRET donor and Cy5-labeled DMPE as the immobile acceptor for which ratiometric sensitivities of 5–15% per 100 mV were recorded (Gonzalez and Tsien 1997). Using the mobile ion as the donor and lowering its concentration, however, produced rapid bleaching. Nevertheless, because there are multiple benefits to using the mobile voltage sensor as FRET donor, further development of this approach is warranted (Dumas and Stoltz 2005), including the development of a more photostable mobile fluorescent anion.

The loading concentrations of $DiSBAC_2(3)$ and $DiSBAC_4(3)$ oxonols are limited to <20 μM for reasons discussed above. For more hydrophobic oxonols, such as $DiSBAC_6(3)$ which have been used primarily in cell culture, the loading concentrations are much lower (<2 μM) due to their lower aqueous solubility and higher membrane partitioning. Loading concentrations of CC1-DMPE are limited to <20 μM in leech neurons because higher concentrations lowered the input resistance of the neurons (Cacciatore et al. 1999). The use of the modified compounds, CC2-DMPE or CC3-DMPE, allows concentrations of up to 160 μM to be used without significantly reducing membrane resistance.

The voltage dependence of the sensitivity can be fit by the Boltzmann statistics for a two-state system under the influence of a potential (Fig. 6.2C) (Gonzalez and Tsien 1995; Cacciatore et al. 1999). The most linear and sensitive region of this curve lies within the physiological range. As with all VSDs, measured sensitivities vary between cell type and experimental preparation. The largest ratiometric sensitivities of 100–300% per 100 mV have been measured in isolated cell lines using CC2-DMPE and $DiSBAC_2(3)$ (Gonzalez and Maher 2002). The use of faster, more hydrophobic oxonols, $DiSBAC_4(3)$ and $DiSBAC_6(3)$, yield sensitivities of 60–100% per 100 mV and 40–80% per 100 mV, respectively (Table 6.1). This reflects the tradeoff between speed and sensitivity as the hydrophobicity of the voltage sensor increases. Sensitivities are reduced for intact tissues such as a leech ganglion due to background staining. Optimal ratioed sensitivities of leech neurons using CC2-DMPE and $DiSBAC_2(3)$ are 10–20% per 100 mV (Fig. 6.2C) (Cacciatore et al. 1999; Briggman et al. 2005). By comparison, the styryl VSD di-4-ANEPPS had sensitivities in leech neurons of around 0.5% per 100 mV.

6.5 GENETICALLY ENCODED FRET SENSORS

Two major limitations of synthetic membrane potential dyes are poor tissue penetration and indiscriminate cellular staining, both of which produce reduced signal above background. A specific challenge for neuroscience applications is labeling target neurons among non-neuronal cells such as glia. To address these issues, several approaches have been explored and developed that utilize genetically encoded fluorescent proteins (FP). Initial efforts involved creating fusion proteins between FP and voltage-gated ion channels and then expressing the construct in the cell or tissue of interest. One general strategy is to turn membrane potential changes into conformational changes in voltage-dependent ion channels, which is then transduced into optical changes. Examples of such voltage-sensitive proteins include: Shaker potassium channels (Siegel and Isacoff 1997; Guerrero et al. 2002); a sodium channel (Ataka and Pieribone 2002); and the voltage sensor domain (VSD) of Kv2.1 potassium channel (Sakai et al. 2001; Knopfel et al. 2003; see also Chap. 14). Although detectable, the voltage-sensitive fluorescence

changes are small and often have complex kinetics resulting from multiple voltage-dependent conformational changes of the VSD, channel, and FP. With the goals of creating ratiometric probes and increasing the voltage-sensitive fluorescence change, constructs were made to express FP FRET pairs attached to voltage-sensitive proteins. These efforts in combination with using the VSD from a voltage sensor containing phosphase from *Ciona intestinalis* (Ci-VSD) have led to development of new FRET-based genetically encoded probes VSFP2.x (Dimitrov et al. 2007) and Mermaid (Tsutsui et al. 2008). These probes have improved voltage-sensitive fluorescence changes with ratiometric changes of ~10% per 100 mV (Mutoh et al. 2009). Using a VSD rather than modified channel proteins has the advantages of (1) not having a channel pore, with its own ionic fluxes, and (2) VSDs are much smaller proteins, which should make them easier to express in cells.

Another FRET or energy transfer approach is a hybrid system that uses a genetically encoded membrane-bound donor FP that undergoes voltage-sensitive energy transfer with a hydrophobic anion. A hybrid approach has the potential to offer both cellular targeting of the photon acceptor along with the high sensitivity inherent in using a mobile voltage sensor anion. A FRET hybrid approach between Lyn-domain targeted GFP and DiSBAC oxonols produces large voltage-sensitive FRET response in mammalian cells and is compatible with high-throughput screening (Tsien and Gonzalez 2002). Recently, a hybrid voltage sensor (hVOS) was constructed that uses a membrane-targeted GFP as the donor and dipicrylamine (DPA) as the acceptor; this combination has a high sensitivity (34% d*F*/*F*) in neurons (Chanda et al. 2005). DPA translocates across membranes with sub-millisecond speed and is not fluorescent, so it functions as a quencher so that all fluorescence changes are from the FP (Blunck et al. 2006). Although high sensitivity is possible, the optimal DPA membrane surface densities occur at such high concentrations that they cause toxicity or introduce a huge capacitive load to the *Drosophila* antennal lobe neurons (Sjulson and Miesenbock 2008). A second hybrid combination used farnesylated FP and the fluorescent oxonol acceptor $DiBAC_4(5)$ to measure membrane potential changes in the transverse tubular system of skeletal muscle fibers of mice (DiFranco et al. 2007). Both combinations increase the capacitance significantly, although action potential signals were observed with DPA. Progress in molecular biology and FPs has catalyzed the search for genetically encoded fluorescent reporters of membrane potential. Still the technical constraints of recording millisecond changes in intact neuronal systems without significantly perturbing the biological system are very demanding constraints that have yet to be met.

6.6 PHOTOTOXICITY OF FRET INDICATORS

Because oxonols readily photobleach, they are the primary source of bleaching during extended voltage-sensitive FRET recordings, even when they serve as FRET acceptors. One contribution to photobleaching is the photochemical reaction between excited states of the dyes and oxygen to generate reactive singlet oxygen. Because the mobile anion is located within the plasma membrane, singlet oxygen causes cellular toxicity by reacting with unsaturated lipids and proteins within the cell membrane. Evidence that oxonol is the major contributor to photodynamic damage comes from experiments in which cardiomyocytes (Gonzalez and Tsien 1997) and leech neurons (K.L. Briggman, unpublished observation) were stained only with oxonol. Phototoxic effects can be partially mitigated by incubating cells with astaxanthin a lipid-soluble carotenoid-free radical scavenger (Palozza and Krinsky 1992; Gonzalez and Tsien 1997). When applied to cardiomyocytes, astaxanthin increased the usable imaging time by a factor of 10. Astaxanthin has similar beneficial effects to reduce photodamage in second harmonic imaging (Sacconi et al. 2006). A key challenge is to develop additional antioxidant compounds that can more readily be loaded into cells.

6.7 APPLICATIONS OF SYNTHETIC FRET VSDS

FRET VSDs have been used in a variety of cell types with applications including high-throughput pharmacology screens, imaging of single neurons, population imaging of intact nervous systems, multilayered keratinocyte cultures (Burgstahler et al. 2003), and pancreatic islets (Kuznetsov et al. 2005). The primary limitations to using FRET VSDs in complex tissue is being able to deliver uniform and sufficient penetration of the two dye molecules to the target cells while minimizing the nonspecific background staining of non-target cells. Therefore, the most successful applications of FRET VSDs have been in preparations with relatively unhindered access to the cell bodies.

6.7.1 High-Throughput Drug Screening

The use of FRET VSDs has been particularly useful for the characterization of pharmacological compounds on the activity of ion channels and transporters in isolated cell lines (Adkins et al. 2001; Weinglass et al. 2008). Isolated cells are easily stained with the more hydrophobic, fast oxonol derivatives such as $DiSBAC_6(3)$, in part, because they do not need to penetrate into tissue. Because the fast fluorescent dyes are very hydrophobic with essentially no aqueous solubility, they bind to the first membrane they encounter. The combination of high-throughput ratiometric FRET detection in microtiter well plates and parallel electrical stimulation has many potential applications, including the rapid characterization of hundreds of voltage-gated sodium channel antagonists (Bugianesi et al. 2006; Huang et al. 2006). Recently, FRET VSDs have been shown to be compatible with the highly miniaturized 1,536 well plate format with an assay for an inward rectifying potassium channel (Solly et al. 2008).

6.7.2 Monitoring Subthreshold Population Activity

Simultaneous recordings from many neurons in the *Aplysia* abdominal ganglia using the fast oxonol absorption VSD, RH155, demonstrated that population activity can be broad and complex in response to sensory stimuli (Tsau et al. 1994; Wu et al. 1994a, b). FRET VSDs have been used to monitor ongoing network activity in leech segmental ganglia. Because the intrinsic locomotory rhythms in the leech are roughly 1 Hz for swimming and 0.1 Hz for crawling (Kristan et al. 2005), $DiSBAC_2(3)$ is sufficiently fast to capture oscillatory dynamics (Briggman and Kristan 2006). The estimation of the magnitude and phase of the coherence between a recording of the motor output on a motor nerve and optical signals from individual neurons provided a quantitative measure of the neurons active at a particular frequency (Cacciatore et al. 1999). The use of multitaper spectral estimation techniques allowed multiple independent estimates of the coherence to be made which provide an estimate of the significance (Fig. 6.3 and Appendix). Importantly, the phase shift due to the time constant of $DiSBAC_2(3)$ proved to be constant across cell types and could, therefore, be subtracted from the signals from the whole population to determine

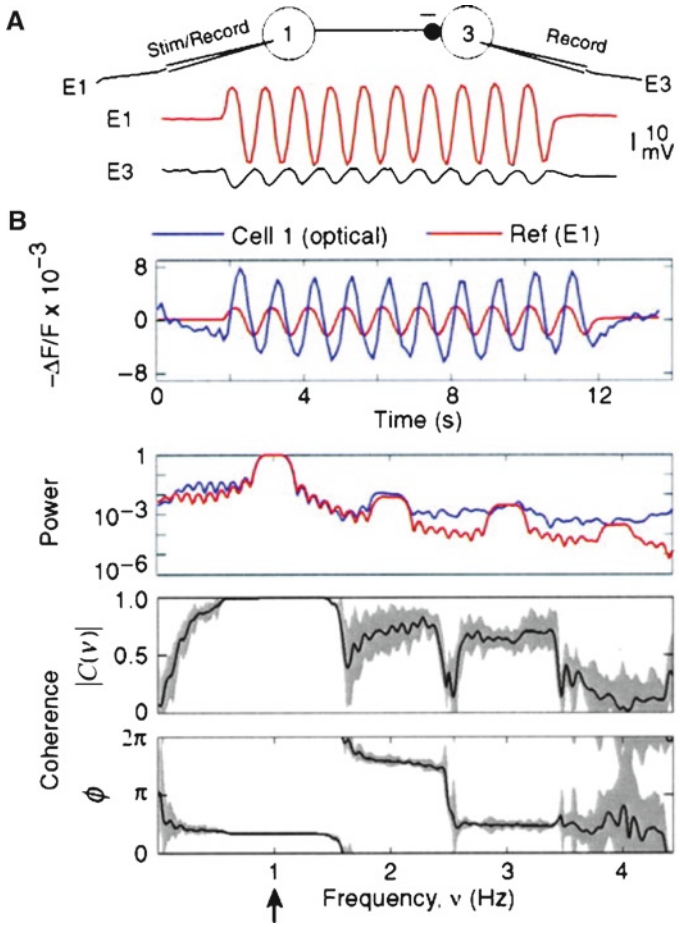

FIGURE 6.3. Coherence-based estimates to characterize optical signals. (A) The membrane potentials of a synaptically connected pair of neurons recorded intracellularly. While stimulating cell 1 with a sinusoidally varying current. E1 and E2 are the recorded membrane potentials of cells 1 and 3. Cell 1 inhibits cell 3. (B) The top trace shows the FRET signal recorded from cell 3, the driven neuron (*black trace*), as its membrane potential was varied sinusoidally (*orange trace*). The significance of the correlation between the optical and underlying electrical signals was quantified by first taking the power spectrum (middle trace). As expected, there were strong peaks at 1 Hz, the frequency that the neuron was driven, and at higher harmonics. The amplitude and phase of the coherence (bottom traces) were then estimated around the primary peak frequency, 1 Hz. The phase of the coherence at this frequency reflects the phase shift caused by the time constant of the oxonol molecule. Panels reproduced with permission from Cacciatore et al. (1999).

accurate phase relationships. This approach led to the identification of novel candidate neurons involved in the swim central pattern generator (CPG).

This work was extended by imaging ongoing leech swimming and crawling in a single preparation (Briggman and Kristan 2006). A direct comparison of the fraction of neurons participating in each of the two behaviors revealed a subpopulation of neurons active during both behaviors. Again, this approach led to the identification of novel, multifunctional neurons that had remained unidentified by electrophysiological methods alone. Non-rhythmic membrane potential changes have also been monitored during the behavioral choice between swimming and crawling (Briggman et al. 2005). The multidimensional analysis of population recordings demonstrated the importance of the ability to resolve signals in single trials and led to the identification of a neuron that can be manipulated to bias the choice between swimming and crawling.

6.7.3 Identifying Functional Connectivity

A particularly useful application of FRET VSDs is the identification of synaptically coupled neurons. The traditional test of functional connectivity, paired electrical recordings from neurons, becomes combinatorially unwieldy as the number of neurons to test increases. An elegant solution to this problem is to drive a presynaptic neuron of interest and use FRET VSDs to image follower neurons (Fig. 6.3A). Because FRET VSDs are sensitive enough to resolve subthreshold fluctuations in membrane potential, it is possible to detect both depolarizing and hyperpolarizing synaptic potentials.

This approach was used to identify postsynaptic targets of a command interneuron, Tr2, located in the head brain of the leech that can terminate swimming (Taylor et al. 2003). A leech segmental ganglion was imaged while Tr2 was driven to produce 1 Hz spike bursts (Fig. 6.4D). The driving frequency of 1 Hz was chosen both to match the time constant of $DiSBAC_2(3)$ and to avoid synaptic fatigue. A recording trial typically contained optical traces from 10 to 20 neurons (Fig. 6.4A–C). The coherence was estimated to identify postsynaptic candidate neurons using the driving signal as reference (Fig. 6.4D, E). Following the rapid screening for postsynaptic follower cells, individual candidate neurons were impaled and connectivity was confirmed by recording spike-evoked postsynaptic potentials in follower neurons. This technique was used to identify two novel neurons postsynaptic to Tr2 that are involved in the termination of the swim CPG.

6.8 ADVANTAGES/DISADVANTAGES

Because of their promiscuous solubility into all cell membranes, FRET VSDs have been used primarily in situations where the somata of neurons are easily accessible to the staining solutions, such as in isolated cells and in invertebrate ganglia. The limited penetration of hydrophobic dyes into complicated neuropil limits the uniformity of staining and nonspecific binding reduces maximal sensitivities. Another inherent disadvantage is the capacitive load introduced by the voltage sensor that can inhibit fast changes in membrane potential such as action potentials. This ultimately limits the usable concentration range of the mobile anion.

A primary advantage of FRET VSDs is the high sensitivity relative to other classes of VSDs. Subthreshold fluctuations in membrane potential down to a few millivolts are resolvable in single trials (Taylor et al. 2003). The slow speed of FRET VSDs is a disadvantage, but the speed is, to some extent, tunable by adjusting the hydrophobicity of the voltage sensor. Hence, the time constant can be matched to the desired application: the slower and more sensitive oxonol derivatives are useful for measuring oscillating and steady state membrane potentials, and the faster versions, including hybrid voltage sensor systems, can be used to monitor action potentials. Because FRET VSDs using fluorescent donors and acceptors are ratiometric, they provide several recording advantages: diminished sensitivities to cell motion artifacts, variation in excitation intensity and donor loading concentration, and the effects of photobleaching. These dyes have become a valuable adjunct to electrophysiological and behavioral studies, to monitor the activity of many neurons while recording electrically from a select few (Marin-Burgin et al. 2005; Baca et al. 2008).

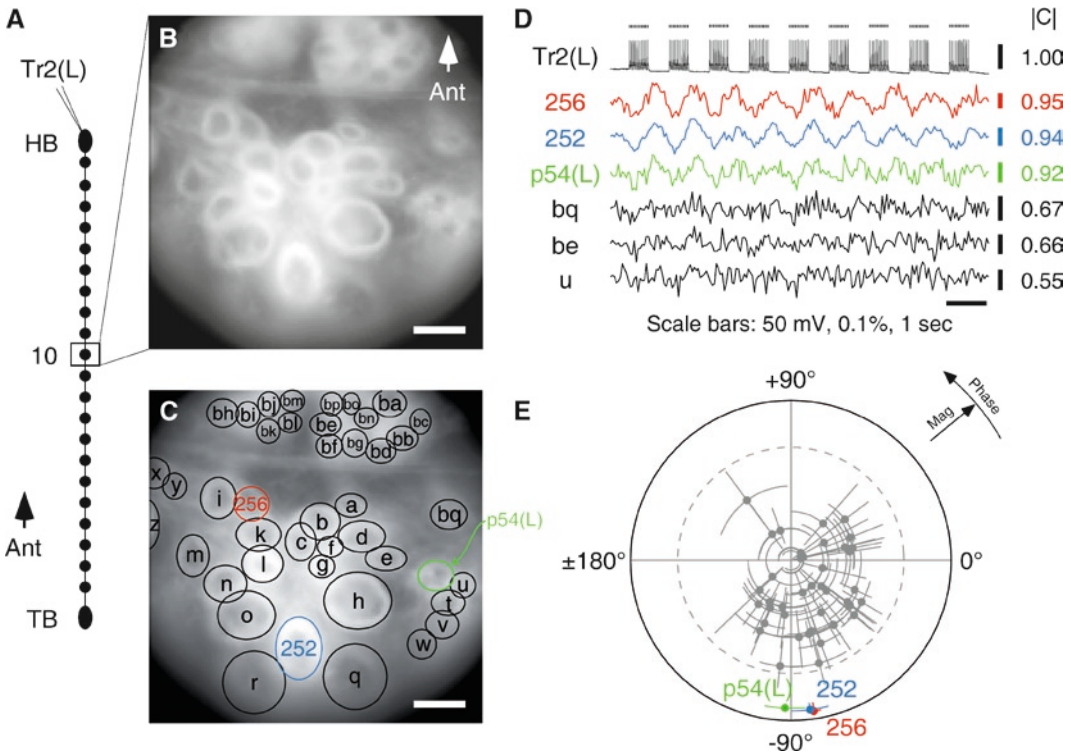

FIGURE 6.4. Identification of synaptic connectivity between neurons. (A) As indicated by the diagram on the left, a neuron (cell Tr2 on the left side) in the head brain (HB) of the isolated leech nerve cord was stimulated while imaging a segmental ganglion. (B) A black/white image of the fluorescence generated by the ventral ganglionic surface stained with the FRET VSDs. (C) Circles drawn around regions of interest – the neuronal somata of many neurons – on the image. (D) Fluorescence changes in six neurons while stimulating cell Tr2. The top trace is a voltage recording from cell Tr2 on the left side of the head brain, indicating when bursts of action potentials were elicited by passing pulses of current into the soma. The remaining traces are optical recordings from six of the cells circled in panel (c). The colored traces showed significant coherence with the action potential bursts in cell Tr2. (E) A polar plot demonstrating the phase and magnitude of the coherence between the stimulated cell and all the optically imaged cells. The dashed line denotes the significance threshold. Panels reproduced with permission from Taylor et al. (2003).

6.9 METHODOLOGICAL DETAILS

6.9.1 Staining Protocol for Leech Segmental Ganglia

1. Pin a desheathed leech segmental ganglion onto a Sylgard coated Petri dish and desheath either the ventral or dorsal surface.
2. Prepare a 30 μM solution of CC2-DMPE by dissolving 3 μl of 5 mM CC2-DMPE in DMSO stock solution (aliquoted and stored at -20°C) and 1 μl of 20 mg/ml pluronic F-127 in DMSO in 500 μl leech saline.
3. Surround the ganglion with a watertight staining chamber consisting of a small plastic cylinder (~1 cm diameter; e.g., the cut end of an Eppendorf tube), sealed to the Sylgard with petroleum jelly. Replace the saline in this chamber with 30 μM CC2-DMPE solution.
4. Stir the staining solution to achieve optimal staining by recirculating the solution using a peristaltic pump. Form a nozzle into the staining chamber by pulling a fine glass microelectrode, breaking off the tip to about a 1 mm diameter, and fire-polishing the tip. Use a dissecting microscope to positioned the nozzle just over the ganglion. Use a glass capillary positioned at the bottom of the chamber for the outflow. Prepare the recirculating system under red light to avoid photobleaching. Stain the ganglion for 30 min in the dark.
5. Rinse the tissue several times with fresh saline.
6. Prepare a 8 μM solution of the selected oxonol (e.g., $DiSBAC_2(3)$) by dissolving 8 μl of oxonol in DMSO stock solution (aliquoted and stored at −20°C) in 12 ml leech saline. Bath sonicate this solution for 2–5 min.
7. Prior to adding the oxonol solution, capture an image of the CC2-DMPE stained ganglion to record the baseline (non-FRET) intensity.
8. Replace the leech saline in the chamber with the oxonol solution. Stain with the oxonol solution for 30 min in the dark. Capture images every 5 min to follow the quenching of the CC2-DMPE fluorescence as the oxonol dissolves into membranes. The quenching of the CC2-DMPE fluorescence stabilizes to ~50% within 30 min.
9. Leave the oxonol solution in the bath during recording, replacing it with fresh solution every 30–60 min.

6.9.2 Staining Protocol for Mammalian Cells in Culture

1. Plate cells grown in flasks or harvested from tissue onto glass coverslips or microtiter plates compatible with fluorescence detection equipment. Allow cells to attach and stabilize in culture at 37°C for 24 h.
2. Wash cells at room temperature with balanced extracellular solution, such as HBSS buffered at pH 7.4.

3. Stain cells for 20–30 min at room temperature with CC2-DMPE (1–20 μM) and oxonol (1–20 μM) solubilized in the extracellular solution, using 0.5% β-cyclodextrin and 20 μg/ml pluronic F-127 as excipients. Prepare dye stock solutions in DMSO from solid material and aliquot into convenient single-use amounts for storage at –20°C. Optimized dye concentrations must be empirically determined because they depend on the specific probe and cell type. Optimize the two dyes by varying their concentrations along the axes of a microtiter plate. On coverslips, optimize the dyes by staining with 10 μM CC2-DMPE, then titrating the oxonol dye while monitoring the CC2-DMPE fluorescence; the optimum oxonol concentration reduces CC2-DMPE fluorescence by 50%. Once optimized, the dyes can be delivered sequentially or simultaneously. Pluronic F-127 assists loading both coumarin DMPE and oxonol dyes; β-cyclodextrin improves the loading of hydrophobic oxonols such as $DiSBAC_6(3)$.
4. Wash away excess dye with a final rinse. For CC2-DMPE and $DiSBAC_6(3)$, the membrane-bound dye remains on plasma membrane for hours at room temperature. The less hydrophobic oxonols like $DiSBAC_2(3)$ will slowly leak out of the cell but this usually does not affect the FRET signal because oxonol is typically used as the acceptor and it is essentially non-fluorescent in water.

6.9.3 Brightfield Imaging Equipment (for Leech Neurons)

Filter set: 405 ± 15 nm bandpass excitation filter; 430 nm dichroic mirror; 460 ± 5 nm bandpass emission filter (for CC2-DMPE); 560 nm longpass emission filter (for $DiSBAC_2(3)$).

Illumination: Tungsten halogen lamp powered by a low-ripple power supply.

Objectives: 40×,0.8 NA or 20×,0.5 NA water immersion objectives.

Camera: A back-illuminated cooled CCD camera. For ratiometric imaging, a second camera is ideal. However, emission-path beam splitters can also been used to record both emission wavelengths with a single camera.

6.9.4 Fluorescent Plate Reader Equipment (for Cultured Cells)

Filter set: 405 ± 7.5 nm bandpass excitation filter; 460 ± 22.5 nm bandpass emission filter (for CC2-DMPE); 580 ± 30 nm bandpass emission filter (for $DiSBAC_x(3)$).

Use appropriate dichroic mirrors as needed for equipment.

Illumination: Xenon arc lamp or other violet source.

Simultaneous ratio detection: trifurcated fiber optic bundles with two-wavelength fluorescence emission detected with PMTs.

APPENDIX

We consider the statistical analysis for determining follower cells (Cacciatore et al. 1999; Taylor et al. 2003; Kleinfeld 2008). The significance of the spectral coherence between the response of any cell, labeled "i", and the driven cell is used to determine if two cells are functionally related and thus are a candidate for a synaptically driven pair. The coherence is a complex function, denoted $C_i(f)$, that it is calculated over the time period of the stimulus, denoted T. We further denote the time series of the optical signals as $V_i(t)$ and the electrical reference drive signal as $U(t)$. The mean value is removed to form:

$$\delta V_i(t) = V_i(t) - \frac{1}{T}\int_0^T \mathrm{d}t V_i(t)$$

with a similar expression for $\delta U(t)$. The Fourier transform of $\delta V_i(t)$ with respect to the kth Slepian window (Thomson 1982; Percival and Walden 1993), denoted $w^{(k)}(t)$, is:

$$\delta\tilde{V}_i^{(k)}(f) = \frac{1}{\sqrt{T}}\int_0^T \mathrm{d}t \mathrm{e}^{-\mathrm{i}2\pi ft} W^{(k)}(t)\,\delta V_i(t)$$

with a similar expression for $\delta\tilde{U}^{(k)}(f)$. The use of multiple tapers allow averaging over a bandwidth that is set by the number of tapers, K, with the half-bandwidth at half-maximal response given by $\Delta f = (1/T)(K+1)/2$. Our interest lies in the values of $C_i(f)$ for $f = f_{\mathrm{Drive}}$ and the confidence limits for these values. We chose the bandwidth so that the estimate of $|C_i(f_{\mathrm{Drive}})|$ is kept separate from that of the harmonic $|C_i(2f_{\mathrm{Drive}})|$. The choice $\Delta f = 0.4 f_{\mathrm{Drive}}$ works well, so that for $f_{\mathrm{Drive}} = 1$ Hz and $T = 9$ s, the integer part of $2 \cdot 0.4 \cdot 1\ \mathrm{Hz} \cdot 9\ \mathrm{s} - 1$ yields $K = 6$ tapers (Fig. 6.3). The spectral coherence between the optical signal and the reference is give by:

$$C_i(f) = \frac{\frac{1}{K}\sum_{k=1}^{K} \delta\tilde{V}_i^{(k)}(f)\left[\delta\tilde{U}^{(k)}(f)\right]^*}{\sqrt{\left(\frac{1}{K}\sum_{k=1}^{K}\left|\delta\tilde{V}_i^{(k)}(f)\right|^2\right)\left(\frac{1}{K}\sum_{k=1}^{K}\left|\delta\tilde{U}^{(k)}(f)\right|^2\right)}}.$$

To calculate the standard errors for the coherence estimates, we use the jackknife (Thomson and Chave 1991) and compute delete-one averages of coherence, denoted $C_i^{(n)}(f)$, where n is the index of the deleted taper:

$$C_i^{(n)}(f) = \frac{\frac{1}{K-1}\sum_{\substack{k=1\\k\neq n}}^{K} \delta\tilde{V}_i^{(k)}(f)\left[\delta\tilde{U}^{(k)}(f)\right]^*}{\sqrt{\left(\frac{1}{K-1}\sum_{\substack{k=1\\k\neq n}}^{K}\left|\delta\tilde{V}_i^{(k)}(f)\right|^2\right)\left(\frac{1}{K-1}\sum_{\substack{k=1\\k\neq n}}^{K}\left|\delta\tilde{U}^{(k)}(f)\right|^2\right)}} \quad \forall n.$$

Estimating the standard error of the magnitude of $C_i(f)$ requires an extra step since $|C_i(f)|$ is defined on the interval [0, 1] while Gaussian variables exist on $(-\infty, \infty)$. Thus the delete-one estimates, $|C_i^{(n)}(f)|$, were replaced with the transformed values:

$$g\left\{|C_i|\right\} = \log\left(\frac{|C_i|^2}{1-|C_i|^2}\right).$$

The mean of the transformed variable is:

$$\mu_{i;\mathrm{Mag}}(f) = \frac{1}{K}\sum_{n=1}^{K} g\left\{C_i^{(n)}(f)\right\}$$

and the standard error of the transformed variable is:

$$\sigma_{i;\mathrm{Mag}}(f) = \sqrt{\frac{K-1}{K}\sum_{n=1}^{K}\left|g\left\{C_i^{(n)}(f)\right\} - \mu_{i;\mathrm{Mag}}(f)\right|^2}.$$

The 95% confidence interval for the coherence is thus:

$$\left[\sqrt{1+\mathrm{e}^{-\left(\mu_{i;\mathrm{Mag}}-2\sigma_{i;\mathrm{Mag}}\right)}}^{-1}, \sqrt{1+\mathrm{e}^{-\left(\mu_{i;\mathrm{Mag}}+2\sigma_{i;\mathrm{Mag}}\right)}}^{-1}\right].$$

We now turn to an estimate of the standard deviation of the phase of $C(f)$. Conceptually, the idea is to compute the variation in

the relative directions of the delete-one unit vectors $C_i(f)/|C_i(f)|$. The standard error is computed as:

$$\sigma_{i;\text{Phase}}(f) = \sqrt{2\frac{K-1}{K}\left(K - \left|\sum_{n=1}^{K}\frac{C_i^{(n)}(f)}{\left|C_i^{(n)}(f)\right|}\right|\right)} \quad \forall n.$$

We graph the magnitude and phase of $C_i(f_{\text{Drive}})$ for all neurons, along with the confidence interval, on a polar plot (Fig. 6.4e). Finally, we consider whether the coherence of a given cell at f_{Drive} is significantly greater than zero, that is, larger than one would expect to occur by chance from a signal with no coherence. We compared the estimate for each value of $|C_i(f_{\text{Drive}})|$ to the null distribution for the magnitude of the coherence, which exceeds

$$\left|C_i\left(f_{\text{Drive}}\right)\right| = \sqrt{1-\alpha^{1/(K-1)}}$$

only in α of the trials (Hannan 1970; Jarvis and Mitra 2001). We use $\alpha = 0.001$ to avoid false-positives. We also calculate the multiple comparisons of α level for each trial, given by $\alpha_{\text{multi}} = 1 - (1 - \alpha)N$, where N is the number of cells in the functional image, and verified that it did not exceed $\alpha_{\text{multi}} = 0.05$ on any trial.

REFERENCES

Adkins CE, Pillai GV et al. (2001) alpha4beta3delta GABA(A) receptors characterized by fluorescence resonance energy transfer-derived measurements of membrane potential. J Biol Chem 276:38934–38939.

Ataka K, Pieribone VA (2002) A genetically targetable fluorescent probe of channel gating with rapid kinetics. Biophys J 82:509–516.

Baca SM, Marin-Burgin A, Wagenaar DA, Kristan WB Jr (2008) Widespread inhibition proportional to excitation controls the gain of a leech behavioral circuit. Neuron 57:276–289.

Baker BJ, Kosmidis EK et al (2005) Imaging brain activity with voltage- and calcium-sensitive dyes. Cell Mol Neurobiol 25:245–282.

Blunck R, Cordero-Morales JF, Cuello LG, Perozo E, Bezanilla F (2006) Detection of the opening of the bundle crossing in KcsA with fluorescence lifetime spectroscopy reveals the existence of two gates for ion conduction. J Gen Physiol 128:569–581.

Briggman KL, Kristan WB Jr (2006) Imaging dedicated and multifunctional neural circuits generating distinct behaviors. J Neurosci 26:10925–10933.

Briggman KL, Abarbanel HD, Kristan WB Jr (2005) Optical imaging of neuronal populations during decision-making. Science 307:896–901.

Bugianesi RM, Augustine PR et al (2006) A cell-sparing electric field stimulation technique for high-throughput screening of voltage-gated ion channels. Assay Drug Dev Technol 4:21–35.

Burgstahler R, Koegel H et al (2003) Confocal ratiometric voltage imaging of cultured human keratinocytes reveals layer-specific responses to ATP. Am J Physiol Cell Physiol 284:C944–C952.

Cacciatore TW, Brodfuehrer PD et al (1999) Identification of neural circuits by imaging coherent electrical activity with FRET-based dyes. Neuron 23:449–459.

Chanda B, Blunck R et al (2005) A hybrid approach to measuring electrical activity in genetically specified neurons. Nat Neurosci 8:1619–1626.

Clegg RM (1995) Fluorescence resonance energy transfer. Curr Opin Biotechnol 6:103–110.

DiFranco M, Capote J, Quinonez M, Vergara JL (2007) Voltage-dependent dynamic FRET signals from the transverse tubules in mammalian skeletal muscle fibers. J Gen Physiol 130:581–600.

Dimitrov D, He Y et al (2007) Engineering and characterization of an enhanced fluorescent protein voltage sensor. PLoS ONE 2:e440.

Dumas D, Stoltz JF (2005) New tool to monitor membrane potential by FRET Voltage Sensitive Dye (FRET-VSD) using Spectral and Fluorescence Lifetime Imaging Microscopy (FLIM). Interest in cell engineering. Clin Hemorheol Microcirc 33:293–302.

Ebner TJ, Chen G (1995) Use of voltage-sensitive dyes and optical recordings in the central nervous system. Prog Neurobiol 46:463–506.

Flewelling RF, Hubbell WL (1986) The membrane dipole potential in a total membrane potential model. Applications to hydrophobic ion interactions with membranes. Biophys J 49:541–552.

Förster VT (1948) Zwischenmolekulare energiewanderung und fluoreszenz. Ann Phys 6:54–75.

Gonzalez JE, Maher MP (2002) Cellular fluorescent indicators and voltage/ion probe reader (VIPR) tools for ion channel and receptor drug discovery. Receptors Channels 8:283–295.

Gonzalez JE, Tsien RY (1995) Voltage sensing by fluorescence resonance energy transfer in single cells. Biophys J 69:1272–1280.

Gonzalez JE, Tsien RY (1997) Improved indicators of cell membrane potential that use fluorescence resonance energy transfer. Chem Biol 4:269–277.

Grinvald A, Ross WN, Farber I (1981) Simultaneous optical measurements of electrical activity from multiple sites on processes of cultured neurons. Proc Natl Acad Sci U S A 78:3245–3249.

Guerrero G, Siegel MS, Roska B, Loots E, Isacoff EY (2002) Tuning FlaSh: redesign of the dynamics, voltage range, and color of the genetically encoded optical sensor of membrane potential. Biophys J 83:3607–3618.

Hannan EJ (1970) Multiple time series. Wiley, New York.

Huang CJ, Harootunian A et al (2006) Characterization of voltage-gated sodium-channel blockers by electrical stimulation and fluorescence detection of membrane potential. Nat Biotechnol 24:439–446.

Jarvis MR, Mitra PP (2001) Sampling properties of the spectrum and coherency of sequences of action potentials. Neural Comput 13:717–749.

Kleinfeld D (2008) Application of spectral methods to representative data sets in electrophysiology and functional neuroimaging. In: Syllabus for Society for Neuroscience Short Course III on "Neural Signal Processing: Quantitative Analysis of Neural Activity", vol 3, Society for Neuroscience, pp 21–34.

Knopfel T, Tomita K, Shimazaki R, Sakai R (2003) Optical recordings of membrane potential using genetically targeted voltage-sensitive fluorescent proteins. Methods 30:42–48.

Kristan WB Jr, Calabrese RL, Friesen WO (2005) Neuronal control of leech behavior. Prog Neurobiol 76:279–327.

Kuznetsov A, Bindokas VP, Marks JD, Philipson LH (2005) FRET-based voltage probes for confocal imaging: membrane potential oscillations throughout pancreatic islets. Am J Physiol Cell Physiol 289:C224–C229.

Lakowicz JR (2006) Principles of fluorescence spectroscopy. Springer, New York.

Maher MP, Wu NT, Ao H (2007) pH-Insensitive FRET voltage dyes. J Biomol Screen 12:656–667.

Marin-Burgin A, Eisenhart FJ, Baca SM, Kristan WB Jr, French KA (2005) Sequential development of electrical and chemical synaptic connections generates a specific behavioral circuit in the leech. J Neurosci 25:2478–2489.

Momose-Sato Y, Sato K et al (1999) Evaluation of voltage-sensitive dyes for long-term recording of neural activity in the hippocampus. J Membr Biol 172:145–157.

Mutoh H, Perron A et al (2009) Spectrally-resolved response properties of the three most advanced FRET based fluorescent protein voltage probes. PLoS ONE 4:e4555.

Palozza P, Krinsky NI (1992) Astaxanthin and canthaxanthin are potent antioxidants in a membrane model. Arch Biochem Biophys 297:291–295.

Percival DB, Walden AT (1993) Spectral analysis for physical applications: multitaper and conventional univariate techniques. Cambridge University Press, New York, NY, USA.

Piston DW, Kremers GJ (2007) Fluorescent protein FRET: the good, the bad and the ugly. Trends Biochem Sci 32:407–414.

Rink TJ, Montecucco C, Hesketh TR, Tsien RY (1980) Lymphocyte membrane potential assessed with fluorescent probes. Biochim Biophys Acta 595:15–30.

Sacconi L, Dombeck DA, Webb WW (2006) Overcoming photodamage in second-harmonic generation microscopy: real-time optical recording of neuronal action potentials. Proc Natl Acad Sci U S A 103:3124–3129.

Sakai R, Repunte-Canonigo V, Raj CD, Knopfel T (2001) Design and characterization of a DNA-encoded, voltage-sensitive fluorescent protein. Eur J Neurosci 13:2314–2318.

Selvin PR (2000) The renaissance of fluorescence resonance energy transfer. Nat Struct Biol 7:730–734.

Siegel MS, Isacoff EY (1997) A genetically encoded optical probe of membrane voltage. Neuron 19:735–741.

Sjulson L, Miesenbock G (2008) Rational optimization and imaging in vivo of a genetically encoded optical voltage reporter. J Neurosci 28: 5582–5593.

Solly K, Cassaday J et al (2008) Miniaturization and HTS of a FRET-based membrane potential assay for K(ir) channel inhibitors. Assay Drug Dev Technol 6:225–234.

Stryer L (1978) Fluorescence energy transfer as a spectroscopic ruler. Annu Rev Biochem 47:819–846.

Taylor AL, Cottrell GW, Kleinfeld D, Kristan WB Jr (2003) Imaging reveals synaptic targets of a swim-terminating neuron in the leech CNS. J Neurosci 23:11402–11410.

Thomson DJ (1982) Spectrum Estimation and Harmonic-Analysis. Proc IEEE 70:1055–1096.

D.J. Thomson and A.D. Chave, Jackknife error estimates for spectra, coherences, and transfer functions, in S. Haykin (ed.), Advances in Spectral Analysis and Array Processing, Englewood Cliffs: Prentice-Hall, pp. 58–113, 1991.

Tsau Y, Wu JY et al (1994) Distributed aspects of the response to siphon touch in *Aplysia*: spread of stimulus information and cross-correlation analysis. J Neurosci 14:4167–4184.

Tsien RY, Gonzalez JE (2002) Detection of transmembrane potentials by optical methods. US Patent 6,342,379 B1.

Tsutsui H, Karasawa S, Okamura Y, Miyawaki A (2008) Improving membrane voltage measurements using FRET with new fluorescent proteins. Nat Methods 5:683–685.

Weinglass AB, Swensen AM et al (2008) A high-capacity membrane potential FRET-based assay for the sodium-coupled glucose co-transporter SGLT1. Assay Drug Dev Technol 6:255–262.

Wu P, Brand L (1994) Resonance energy transfer: methods and applications. Anal Biochem 218:1–13.

Wu JY, Cohen LB, Falk CX (1994a) Neuronal activity during different behaviors in *Aplysia*: a distributed organization? Science 263:820–823.

Wu JY, Tsau Y et al (1994b) Consistency in nervous systems: trial-to-trial and animal-to-animal variations in the responses to repeated applications of a sensory stimulus in *Aplysia*. J Neurosci 14:1366–1384.